Use of a low pressure helium/water vapor discharge as a mercury-free source of ultraviolet emission

ARTICLE *in* JOURNAL OF APPLIED PHYSICS · SEPTEMBER 2014

Impact Factor: 2.18 · DOI: 10.1063/1.4896188

5 AUTHORS, INCLUDING:

Dmitry Levko

University of Texas at Austin

66 PUBLICATIONS **248** CITATIONS

SEE PROFILE

A. Tsymbalyuk

Taras Shevchenko National University of Kyiv

6 PUBLICATIONS **12** CITATIONS

SEE PROFILE

AIP | Journal of Applied Physics

Use of a low pressure helium/water vapor discharge as a mercury-free source of ultraviolet emission

Dmitry Levko, Alexander Shuaibov, Igor Shevera, Roksolana Gritzak, and Alexander Tsymbaliuk

Citation: Journal of Applied Physics **116**, 113303 (2014); doi: 10.1063/1.4896188
View online: http://dx.doi.org/10.1063/1.4896188
View Table of Contents: http://scitation.aip.org/content/aip/journal/jap/116/11?ver=pdfcov
Published by the AIP Publishing

Use of a low pressure helium/water vapor discharge as a mercury-free source of ultraviolet emission

Dmitry Levko,[1] Alexander Shuaibov,[2] Igor Shevera,[2] Roksolana Gritzak,[2] and Alexander Tsymbaliuk[3]
[1]*LAPLACE (Laboratoire Plasma et Conversion d'Energie), Universite de Toulouse, UPS, INPT Toulouse, 118 route de Narbonne, F-31062 Toulouse Cedex 9, France*
[2]*Department of Quantum Electronics, Uzhgorod National University, Pidhirna Str. 46, 88000 Uzhgorod, Ukraine*
[3]*Department of Physics, East Ukrainian Vladimir Dahl National University, Molodizhnyi kvartal 20-a, 91034 Lugansk, Ukraine*

(Received 25 June 2014; accepted 9 September 2014; published online 19 September 2014)

This paper presents the results of study of the longitudinal low-pressure glow discharge in a helium/water mixture. This discharge is proposed for use as a mercury-free source of ultraviolet emission. The emission spectra in the ultraviolet range are recorded by a monochromator and analyzed. In order to interpret the experimental results, the numerical modeling is carried out using global model for 46 species and 577 plasma chemical reactions between them. This model allows us to define the main reactions responsible for the generation and quenching of the excited species, which emit in the ultraviolet range. The optimal conditions are found when the lines with wavelengths of 309 nm OH(A-X) and 150–190 nm OH(X-C,B) have the largest intensity.
 [http://dx.doi.org/10.1063/1.4896188]

I. INTRODUCTION

Nowadays, the use of water vapors in ultraviolet (UV) and vacuum ultraviolet (VUV) gas discharge lamps attracts a lot of attention due to the possibility to work with non-toxic and cheap medium.[1–12] The use of water vapors allows the efficient generation of excited radicals OH, whose spontaneous emission has a wavelength of 309 nm. In perspective, these lamps can replace traditional excimer XeCl and mercury VUV-UV lamps.

During the last decade, the light emission from low-pressure plasmas generated in the pure water vapors or in their mixtures with different rare gases (Ne, Ar, Kr or He) was extensively studied.[1–12] The possibility to develop cheap and environmentally clean VUV-UV lamps based on the longitudinal glow discharges in low-pressure He/H_2O and Ar/H_2O mixtures has been demonstrated.[1,2] Experimental results have shown that the main emission line is the line of OH(A–X;0–0), whose wavelength is $\lambda = 306.4$ nm. Pulsed-periodic capacitive discharge in the pure water vapors for UV emission with $\lambda = 309$ nm was studied in Ref. 7. Experimental results presented in Ref. 9 have shown that an admixture of He to H_2O increases the electron temperature 1.5–2 times in comparison with the discharge in pure H_2O. Thus, the efficiency of active species generation also increases, which results in the increase in the intensity of UV emission.

Artamonova *et al.*[5,6] studied the spectral and electrical characteristics of a low-pressure direct current discharge initiated in the mixtures of H_2O with Ne, Ar, or Kr. It was found that the use of Ar is more profitable than the use of Ne and Kr. Authors concluded that the most probable process of OH(A) generation is the quenching of excited states of argon by the collisions with water molecules.

The VUV emission of the nanosecond low-pressure discharge in He/H_2O and Ar/H_2O mixtures was studied in Refs. 10 and 11. The electron kinetic coefficients were calculated for Ar/H_2O mixture. In addition, the emission lines of cluster molecules,[13] such as $(OH)_n$, $(H_2O)_m$, and $Ar_n{\cdot}(H_2O)_m$ (n, m $\geq$ 1), were registered.

The physical processes in a low-pressure barrier discharge lamp working in the mixture of He with "heavy" water (D_2O) were studied in Ref. 12. It was found that the intensity of UV emission is the non-monotonic function of D_2O and He pressures. In addition, the influence on the plasma parameters of the discharge voltage and frequency of the discharge pulses was studied in detail.

In spite of these researches, many open questions still remain. First, the optimal conditions for VUV-UV and visible light emission are not found yet. Second, the intensity and emission spectra of the lamp based on water molecules require detailed study for a wide range of parameters. Finally, the processes responsible for the generation and quenching of the excited species emitting in the VUV-UV range require detailed theoretical analysis. All these questions will be addressed in the present paper. In particular, the optimization of the output characteristics of the glow discharge lamp using the H_2O/He mixture is performed for the first time. It is found that the use of He/H_2O mixture is more perspective than the use of pure H_2O. The experimental results are interpreted using the global model simulations. These simulations allow us to define the main processes responsible for the generation and quenching of excited species, which emit in the VUV-UV range.

II. EXPERIMENTAL CONDITIONS AND DIAGNOSTICS

In this study, we use He/H_2O mixture and pure H_2O. The experiments are carried out for the water vapor pressure in the range 0.05–0.15 kPa. The gas is at the room temperature (300 K). The longitudinal glow discharge is initiated in

the quartz tube (model KY-2). The distance between electrodes is 5 cm and the tube inner radius is 0.35 cm. The residual air pressure in the camera does not exceed 10–15 Pa.

The discharge tube is connected with a vacuum monochromator through the window made of CaF_2 (Fig. 1). Thus, the one end of the quartz tube is in front of the monochromator slot, which is equipped by the photomultiplier having LIF window (FEU-142). This enables the analysis of the discharge emission in the spectral range 140–315 nm. Emission in the spectral range 200–800 nm is analyzed by the monochromator MDP-2 and photomultiplier FEU-106. The spectral resolution of the vacuum monochromator does not exceed 0.7 nm.

The spectral line intensity is calculated by the area under the corresponding spectral curve. This intensity is corrected taking into account the relative spectral sensitivity of the both monochromator and photomultiplier. The accuracy of measurements does not exceed 7–10%. The longitudinal discharge current is in the range 2–50 mA, and the electric power is in the range 40–60 W.

III. ELECTRICAL AND OPTICAL CHARACTERISTICS OF DISCHARGE

The experimental results have shown that the longitudinal homogeneous glow discharge is initiated for the water vapor pressure in the discharge tube of $p(H_2O) = 50–300$ Pa and the helium pressure of $p(He) = 2–6$ kPa. This discharge has a white color and uniformly fills the space between electrodes. The breakdown voltage is in the range 0.9–1.25 kV and the steady-state discharge voltage is $U_d = 0.85–0.9$ kV. The discharge current is $I_d \geq 25$ mA. It is obtained that an admixture of He to H_2O leads to the increase in both the breakdown and steady-state voltages.

The emission spectrum of the glow discharge registered in the experiments is shown in Fig. 2. The experimental results show that the main emission lines at $p(H_2O) = 50–300$ Pa in the VUV-UV range are the lines having wavelengths $\lambda = 156$, 180, and 186 nm. The increase in $p(H_2O)$ up to the value of saturated vapors results in the decrease in the emission intensity and results in the broadening of the lines. The latter leads to the overlapping of these lines. At these conditions, the main lines are lines with $\lambda = 313$ nm and 286 nm (Fig. 2).

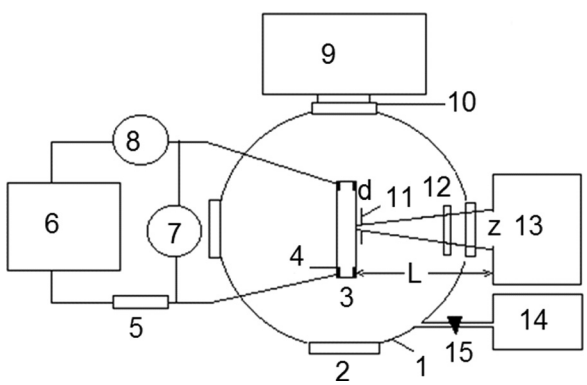

FIG. 1. Schematic of the experimental setup: 1, discharge chamber; 2, quartz windows; 3, discharge tube; 4, electrodes; 5, ballast resistance 0.4–0.5 MΩ; 6, high voltage rectifier; 7, milliammeter; 8, kilovoltmeter; 9, vacuum spectrometer; 10, MgF_2 window; 11, aperture; 12, filter; 13, the power meter of emission "Quartz 01;" 14, vacuum and gas mixing system; 15, vacuum truck.

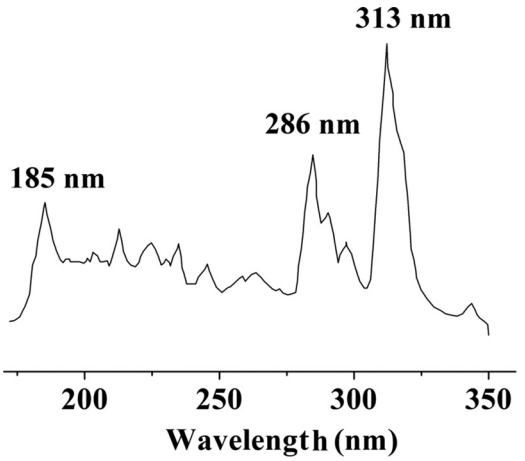

FIG. 2. VUV-UV emission spectrum of the longitudinal glow discharge in the water vapors at $p(H_2O) = 0.05–0.15$ kPa; $I_d = 50$ mA.

The analysis of emission spectra shows that the main excited specie emitting in the VUV-UV range at the given conditions is the radical OH(A-X;0–0). This specie is generated due to the water dissociation by the electron impact. The quenching of OH(A-X;0–0) is accompanied by the emission having wavelength of 306.4–308.9 nm.

In addition, the experiments are carried out in the pure unsaturated water vapors. It is obtained that the edge at $\lambda = 180$ nm coincides with the edge of line OH(C-A), which has $\lambda = 179.1$ nm. The line having the smallest wavelength of 156 nm can be associated with the system of line OH(B-X).[14] The increase in $p(H_2O)$ results in the drastic decrease in intensity of the line with $\lambda = 156$ nm, while the system of the lines with $\Delta\lambda = 180–186$ nm transforms into one broad line having $\lambda = 186$ nm.

The broad line having a maximum at $\lambda = 286$ nm correlates with the edges of lines 282.9 nm OH(A-X;1–0) and 278 nm OH(B-A). The edge of line having a maximum at $\lambda = 262$ nm correlates with the edge 262.2 nm OH(A-X;2–0). The continuum is possible due to the presence of hydrogen-like clusters and emission of the hydrogen molecule.

In addition, our experimental results show, the presence in the discharge spectra, not only well known lines of radical OH(A-X;C-A), but also the presence of other broad lines. These lines can be associated with the presence in the mixture of cluster molecules, such as $(OH)^*_n$, $(OH)^*\cdot(H_2O)_m$, and $He_n\cdot(H_2O)_m$. Zavilopulo *et al.*[13] discussed that these clusters can be generated in discharges in the mixtures of rare gases with molecular gases.

Water molecule has a big dipole moment. Therefore, the rate coefficients of reactions leading to the generation of clusters are expected to be large. As a consequence, the large densities of cluster molecules are expected at high water vapor pressure. The presence of such clusters makes possible the reaction $e + (H_2O)_n \rightarrow H^-\cdot(H_2O)_{n-1} + OH^*$ leading to the generation of excited hydroxyl radical. Thus, the possible mechanism of emission with $\lambda = 309.6$ nm registered in our experiments can be the following. The collision between two or three OH* radicals leads to the generation of $(OH)^*_n$ and

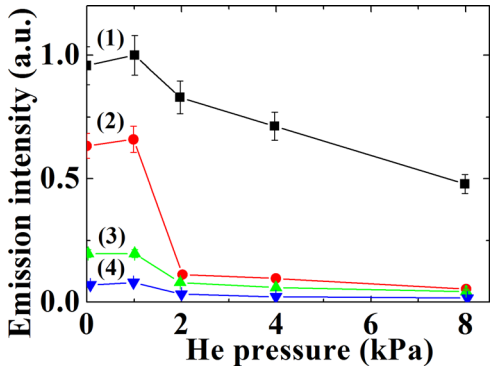

FIG. 3. Dependence on the helium pressure of intensity of the characteristic lines of the glow discharge in He/H_2O mixture for $p(H_2O) = 100$–150 Pa and $I_d = 50$ mA: (1) $\lambda = 180 + 186$ nm, (2) 156 nm, (3) 313 nm, and (4) 286 nm.

$(OH)^*_n \cdot (H_2O)_m$ ($n \geq 2$, $m \geq 1$). This process is accompanied by the decrease in the energy of the highest electronic state and by the shift of the emission line edge to the long wavelength region of the spectrum.

In order to find the optimal conditions of the lamp, the experiments are carried out in a wide range of the water and helium pressures. These results are summarized in Fig. 3 and Table I. It is found that the intensity of emission lines of excited OH significantly depends on p(He). The stronger influence of $p(H_2O)$ on the intensity of lines having smaller wavelength is also obtained. The experimental results show (Fig. 3) that the optimal partial pressure of He, which is necessary for the maximum intensity of the lines 156, 180, and 186 nm, is ≈1.0 kPa [$p(H_2O) = 100$–150 Pa]. In addition, the linear dependence of intensity on the discharge current is measured for all studied pressures. This indicates on the direct population of the energetic levels by the electron impact. In Sec. V, these results will be analyzed by the numerical modeling.

IV. NUMERICAL MODEL

In order to analyze the plasma chemical processes during the discharge, the numerical modeling is carried out using the global (zero-dimensional) model. The following system of kinetic equations is solved each time step until the species densities reach the steady-state values:

$$\frac{dn_m}{dt} = S_m - \frac{D}{\Lambda^2} \cdot n_m. \quad (1)$$

Here, n_m is the density of mth specie (electrons, ions and neutrals), S_m is the term describing the generation and decay of mth specie due to the plasma chemical reactions, and $m \in [1, N_{\max}]$, where N_{max} is the total number of species considered in the model. In Eq. (1), D is the diffusion coefficient and Λ is the characteristic diffusion length. For cylindrical tube, it is $1/\Lambda^2 = (2.4/R)^2 + (\pi/L)^2$, where R is the tube inner radius (0.35 cm) and L is the distance between electrodes (5 cm).

TABLE I. Intensity of the characteristic lines of the glow discharge at different water pressures.

λ, nm	156 OH(B-X)	180–186 OH(C-A)	286 OH(A-X; 1-0)	306–315 OH(A-X; 0-0)
I, a.u. $p(H_2O) = 0.1$ kPa	610	920	54	90
I, a.u. $p(H_2O) = 2.5$ kPa	≤ 1	4	10	32

The term describing the generation and decay is calculated by

$$S_m = \sum_r C_{m,r} R_r. \quad (2)$$

Here, $C_{m,r}$ is the total number of species p created in one reaction event of type r; its value is either positive (generation) or negative (decay). Also, R_r is the reaction rate of type r. For instance, for two-body reaction having rate coefficient k, it is calculated as $R_r = k_{r,1,2} \cdot n_1 n_2$.

At $t = 0$, the electron density is calculated by

$$n_{e0} = \frac{W_d/V}{W_{in} + W_{el}}. \quad (3)$$

This density is kept constant during the modeling. In Eq. (3), W_d is the discharge power, whose value is taken from the experiments, V is the discharge volume, W_{in} and W_{el} are, respectively, the power spent in inelastic and elastic electron-neutral collisions

$$W_{in} = \sum k_{in} \varepsilon_{in} N_g, \quad (4)$$

$$W_{el} = 3 m_e T_e \sum \frac{N_g k_{el}}{M}. \quad (5)$$

In Eq. (4), the sum is taken over all inelastic reactions between electrons and He or H_2O. These reactions have rate coefficients k_{in} and energy thresholds ε_{in}. In Eq. (5), m_e is the electron mass, T_e is the electron temperature, and M is the mass of He or H_2O. In this equation, the sum is taken over all elastic electron-neutral reactions, which have rate coefficients k_{el}.

Rate coefficients of elastic and inelastic reactions are calculated using the electron energy distribution function (EEDF). The EEDF is calculated by the numerical solution of the Boltzmann kinetic equation in the two-term approximation. Only the electron-H_2O and electron-He collisions are taken into account for the EEDF calculation. The list of these reactions can be found elsewhere.[12,15] The electron temperature is defined as $T_e = 2/3\langle\varepsilon_e\rangle$, where $\langle\varepsilon_e\rangle$ is the average electron energy.

Diffusion coefficients of positive ions in Eq. (1) are defined as $D_i = \pi \cdot v_i \cdot \lambda_i/8$, where $v_i = \sqrt{8k_B T/\pi M_i}$ is the ion thermal velocity, k_B is the Boltzmann constant, T is the gas temperature (300 K), M_i is the ion mass, and $\lambda_i = 1/(N_g \pi (R_{H_2O} + R_{He})^2)$ is the ion mean free path. Also, R_{H_2O} and R_{He} are the radii of H_2O and He, respectively. The neutral diffusion coefficients are calculated in analogy to the ion diffusion coefficients for the neutral velocity $v_i = \sqrt{2k_B T/M_i}$.

Diffusion coefficients of negative ions are assumed equal to zero because plasma sheath potential near the electrodes is much larger than the ion temperature. Therefore, negative ions cannot escape the plasma. The total set of

plasma chemical reactions is taken from Ref. 15. It includes 46 species (electrons, positive and negative ions, atoms, and radicals in the ground and excited states) with 577 reactions between them. This scheme is of interest because it takes into account OH(A), H(n = 2), H(n = 3), and He*, which are the subject of our research.

V. RESULTS OF NUMERICAL MODELING AND COMPARISON WITH THE EXPERIMENTAL RESULTS

The modeling is carried out for $p(\mathrm{He}) = 1$–$9\,\mathrm{kPa}$, $p(\mathrm{H_2O}) = 50$–$300\,\mathrm{Pa}$, $I_d = 50$–$300\,\mathrm{mA}$, and $U_d = 1\,\mathrm{kV}$. These parameters correspond to the experimental conditions described in Secs. II and III.

Fig. 4 shows the temporal evolution of the densities of excited species and OH obtained for $p(\mathrm{He}) = 1\,\mathrm{kPa}$, $p(\mathrm{H_2O}) = 150\,\mathrm{Pa}$, $U_d = 1\,\mathrm{kV}$, and $I_d = 40\,\mathrm{mA}$. One can see that He* has the largest density among excited species. This is caused by the fact that the He density is almost one order of magnitude larger than the density of H_2O, which is the source of other active species shown in Fig. 4.

The results of modeling show that the main channel of OH(A) generation is the reaction

$$\mathrm{e} + \mathrm{H_2O} \rightarrow \mathrm{e} + \mathrm{H} + \mathrm{OH(A)}. \quad (6)$$

This reaction is the dominant process for all helium-to-water ratios studied in the present paper. The second order reaction leading to OH(A) generation is the following:

$$\mathrm{e} + \mathrm{OH} \rightarrow \mathrm{e} + \mathrm{OH(A)}. \quad (7)$$

Model results show that the increase in $p(\mathrm{He})$ leads to the decrease in the ratio between rates of reactions (6) and (7). For instance, at $p(\mathrm{He}) = 1\,\mathrm{kPa}$ and $p(\mathrm{H_2O}) = 150\,\mathrm{Pa}$ $k_6/k_7 \approx 16$, and at $p(\mathrm{He}) = 9\,\mathrm{kPa}$ and $p(\mathrm{H_2O}) = 150\,\mathrm{Pa}$ $k_6/k_7 \approx 3$. The opposite effect is obtained for increasing water pressure. For instance, at $p(\mathrm{He}) = 1\,\mathrm{kPa}$ and $p(\mathrm{H_2O}) = 300\,\mathrm{Pa}$, one gets $k_6/k_7 \approx 23$.

Because in He/H_2O mixture OH(A) radicals are generated in the direct electron impact dissociation reaction (6), the use of this mixture is more energy efficient than the use of Ar/H_2O. The largest conversion efficiency of UV photon to the visible region in Ar/H_2O is estimated as 0.18. Following the same method, one can estimate the largest efficiency in He/H_2O mixture as $1/2 \cdot \varepsilon[\mathrm{OH(A)}]/\varepsilon_6 \approx 0.23$, where $\varepsilon[\mathrm{OH(A)}] = 4.1\,\mathrm{eV}$ and $\varepsilon_6 \approx 9\,\mathrm{eV}$ is the energy threshold of reaction (6).

The densities of excited species and OH in the ground state as the functions of helium pressure are shown in Fig. 5. Also, Fig. 5(c) shows the influence of p(He) on EEDF. One can see that the increase in p(He) (U_d is kept constant) leads to the decrease in the electron number in the high-energy tail of EEDF. This results in the decrease in the average electron energy and, as a consequence, in the decrease in the electron temperature. The latter results in the decrease in the rates of electron-neutral reactions (6) and (7), which consequently results in the decrease in the density of OH(A). In addition,

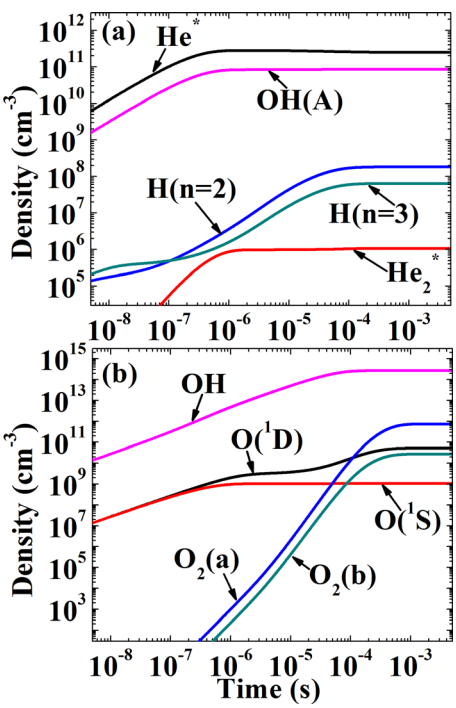

FIG. 4. Time dependence of the densities of excited species; $p(\mathrm{He}) = 1\,\mathrm{kPa}$, $p(\mathrm{H_2O}) = 150\,\mathrm{Pa}$, $U_d = 1\,\mathrm{kV}$, and $I_d = 40\,\mathrm{mA}$.

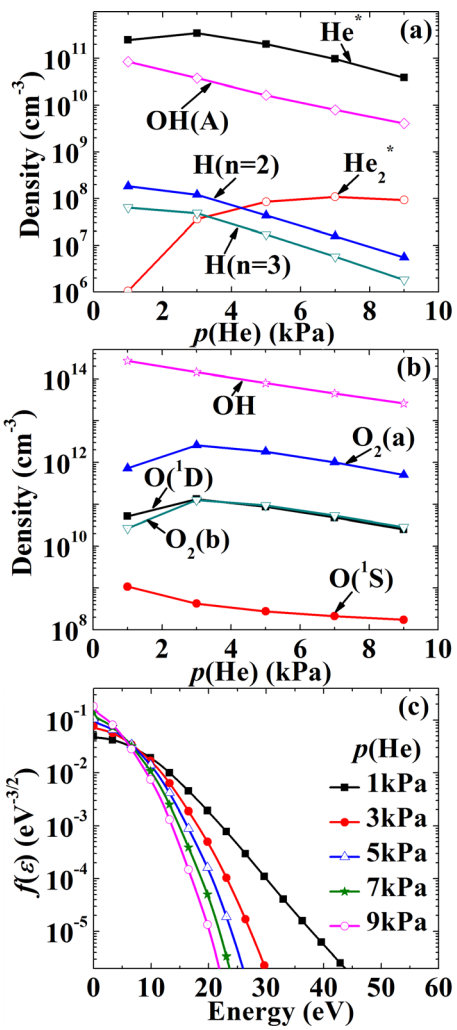

FIG. 5. (a) and (b) Densities of excited species and OH; (c) electron energy distribution function as the function of helium pressure; $p(\mathrm{H_2O}) = 150\,\mathrm{Pa}$, $U_d = 1\,\mathrm{kV}$, and $I_d = 40\,\mathrm{mA}$.

the model results show that the increase in p(He) causes the change of reactions responsible for the quenching of OH(A). Namely, at p(He) < 1 kPa, quenching occurs in reaction

$$OH(A) + H_2O \rightarrow OH + H_2O. \quad (8)$$

The second order quenching reaction is the spontaneous emission

$$OH(A) \rightarrow OH + h\nu. \quad (9)$$

At p(He) > 1 kPa, the dominant quenching reaction of OH(A) is reaction (9). Rate coefficients of (8) and (9) do not depend on the electron temperature. Therefore, the switching between (8) and (9) is explained by the dependence of the steady-state value of the H_2O density on p(He).

Fig. 5 shows the insignificant influence of p(He) on the ratio between densities of H(n = 2) and H(n = 3). This ratio is ≈4. Therefore, the ratio between intensities of these lines does not depend on p(He) as well. This ratio can be calculated as

$$\frac{I[H(n=2)]}{I[H(n=3)]} = \frac{\lambda_3}{\lambda_2}\frac{A_2}{A_3}\frac{n[H(n=2)]}{n[H(n=3)]}. \quad (10)$$

Here, $\lambda_{2,3}$, $A_{2,3}$, and n[H(n = 2,3)] are the wavelength, transition probability, and density of H(n = 2) and H(n = 3), respectively. Using $A_2 = 4.41 \times 10^7\ s^{-1}$ and $A_3 = 8.42 \times 10^6\ s^{-1}$, one finds that $I[H(n=2)]/I[H(n=3)] \approx 16$, which is in satisfactory agreement with the experimental results (see Table I).

Fig. 5(b) shows the largest value of OH density $\sim 3 \times 10^{14}\ cm^{-3}$. At the same time, the density of water vapors is $3 \times 10^{16}\ cm^{-3}$, i.e., it is much larger than the density of OH. Thus, one can assume that the generation of highly excited OH occurs due to the dissociation of H_2O by the electron impact. Nowadays, the cross sections of these reactions are not known. Nevertheless, they can be estimated from the known cross section of reaction (6) as the following:

$$\sigma_2 \approx \sigma_1 \cdot \varepsilon_1/\varepsilon_2 = \sigma_1 \cdot \lambda_2/\lambda_1. \quad (11)$$

Here, σ_1, ε_1, and λ_1 are the cross section, energy threshold, and wavelength of reaction (6), respectively, and σ_2, ε_2, and λ_2 are those ones of highly excited states. In addition, one can assume that the density of highly excited state of OH is proportional to the cross section. Fig. 5(a) shows that at $p(H_2O) = 150$ Pa and p(He) = 1 kPa, one has $n[OH(A)] \approx 10^{11}\ cm^{-3}$. Then, one obtains n[OH(C-A)] ≈ $5.8 \times 10^{10}\ cm^{-3}$ and n[OH(B-X)] ≈ $5.2 \times 10^{10}\ cm^{-3}$. Equation (11) also shows that the dependence of the densities (intensities) of the highly excited states on the external parameters is similar with that obtained for OH(A). Namely, the increase in p(He) results in the decrease in the emission intensity.

The ratio between intensities of H(n = 2) and OH(A) can be calculated as[10]

$$\frac{I[OH(A)]}{I[H(n=2)]} = \frac{\lambda_2}{\lambda(OH)}\frac{1/\tau}{A_2}\frac{n[OH(A)]}{n[H(n=2)]}. \quad (12)$$

Here, τ is the life time of the first excited state of OH, which is the reciprocal of the rate coefficient of reaction (9) $k = 1.25 \times 10^6\ s^{-1}$. Then, $I[OH(A)]/I[H(n=2)] = 0.06 \cdot n[OH(A)]/n[H(n=2)]$. At $p(H_2O) = 150$ Pa and p(He) = 1 kPa, one obtains $n[OH(A)] \approx 10^{11}\ cm^{-3}$ and $n[H(n=2)] \approx 2 \times 10^8\ cm^{-3}$. Thus, $I[OH(A)]/I[H(n=2)] \approx 30$.

The influence of the water pressure on the densities of excited species and OH, and EEDF is shown in Fig. 6. Fig. 6(c) shows that the increase in $p(H_2O)$ results in the decrease in the electron number in the high-energy tail of EEDF. This results in the decrease in the electron temperature. One can therefore conclude that the increase in $p(H_2O)$ results in the decrease in the rate coefficients of reactions (6) and (7). However, rates of reactions (6) and (7) grow due to the increase in the density of H_2O. In addition, model results show that for all considered values of $p(H_2O)$, the main quenching reaction of OH(A) is reaction (8), whose rate increases when $p(H_2O)$ increases. Model results also show [Fig. 6(a)] that the density of H(n = 3) insignificantly depends on the water pressure, while the density of H(n = 2) increases for increasing $p(H_2O)$. Thus, the increase in $p(H_2O)$ results in the increase in intensity of H(n = 3).

The influence of the discharge current on the species densities is shown in Fig. 7 (U_d is kept constant). One can

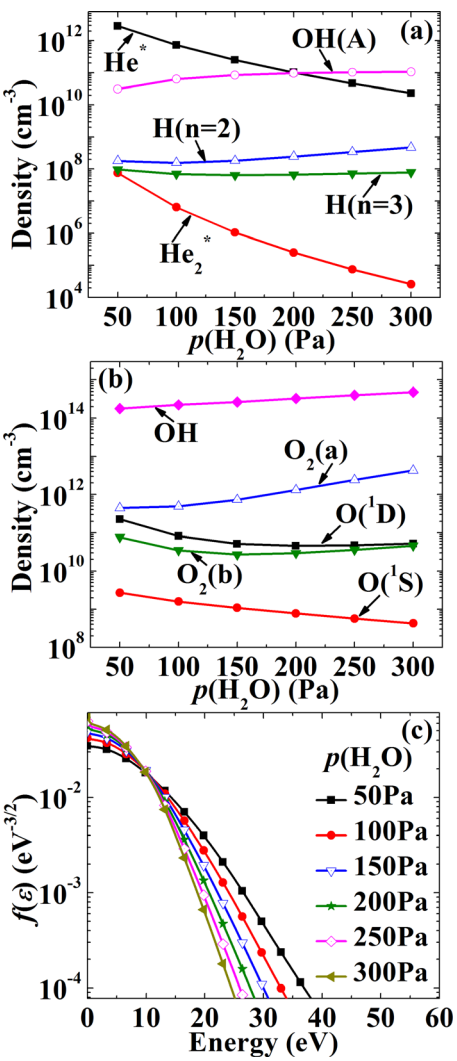

FIG. 6. Influence of the water pressure on the densities of excited species and OH (a) and (b) and on the electron energy distribution function (c); p(He) = 1 kPa, U_d = 1 kV, I_d = 40 mA.

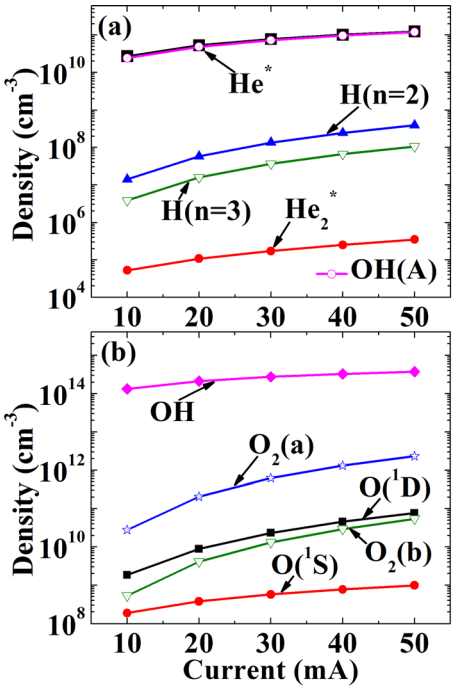

FIG. 7. Influence of the discharge current on the densities of excited species and OH; $p(\mathrm{He}) = 1$ kPa, $p(\mathrm{H_2O}) = 200$ Pa, $U_d = 1$ kV.

see that the increase in I_d results in the linear increase in the densities of all species. This is caused by the fact that the increase in I_d results in the linear increase in the discharge power, which in accordance with Eq. (3) results in the linear increase in the electron density. As a consequence, the rates of electron-neutral reactions are also the linear functions of power.

Finally, let us estimate the power of UV emission of OH(A) as

$$P = n[\mathrm{OH(A)}] \cdot V \cdot q_e \cdot \varepsilon[\mathrm{OH(A)}] \cdot k. \qquad (13)$$

Here, $V = 1.9\,\mathrm{cm}^{-3}$ is the discharge tube volume, q_e is the elementary charge, and k is the rate coefficient of quenching reaction (9). Substituting $k = 1.25 \times 10^6\,\mathrm{s}^{-1}$ and $n[\mathrm{OH(A)}] \approx 10^{11}\,\mathrm{cm}^{-3}$, one gets $P \approx 0.16$ W. Taking into account that the discharge power is 50 W, one concludes that only 0.3% of electrical power goes into the UV emission of OH(A) radical.

VI. CONCLUSIONS

The longitudinal low-pressure glow discharge in the helium/water mixture was studied experimentally and by numerical zero-dimensional model. It is expected that this discharge can be used as the efficient mercury-free source of the ultraviolet emission.

The experimental results have shown that at low water pressure ($\leq$300 Pa), the discharge in $\mathrm{He/H_2O}$ mixture is the efficient source of vacuum ultraviolet emission having wavelengths of 157, 180, and 186 nm.

The numerical modeling allowed us to define the chemical composition of the gas mixture as well as the main channels of the generation and quenching of excited species. It was obtained that at the considered conditions, the main excited specie is He*. However, the density of OH(A) was comparable with the density of He*. The main product of water dissociation was the radical OH in the ground state. Also, the model results showed that the main channel of OH(A) quenching significantly depends on the helium pressure.

Thus, our results have shown the possibility of the development of ecologically clean VUV-UV lamp working on the longitudinal low-pressure glow discharge in $\mathrm{He/H_2O}$ mixture. Nowadays, we are working on the increase in the energy efficiency and intensity of this lamp.

[1]A. Vul', S. Kidalov, V. Milenin, N. Timofeev, and M. Khodorkovskii, Tech. Phys. Lett. **25**, 4 (1999).
[2]A. Vul', S. Kidalov, V. Milenin, N. Timofeev, and M. Khodorkovskii, Tech. Phys. Lett. **25**, 321 (1999).
[3]J. Kornev, N. Javorovskij, G. Ivanov, G. Savel'ev, and T. Shamanskaja, Izv. Tomsk. Politeh. Univ. **306**, 78 (2003).
[4]A. Shuaibov, L. Shimon, A. Dashchenko, and I. Shevera, Proc. SPIE **4747**, 409 (2002).
[5]E. Artamonova, T. Artamonova, A. Beliaeva, D. Gorbov, M. Khodorkovskii, A. Melnikov, D. Michael, V. Milenin, S. Murashov, L. Rakcheeva, and N. Timofeev, J. Phys. D: Appl. Phys. **41**, 155206 (2008).
[6]E. Artamonova, T. Artamonova, A. Beliaeva, M. Khodorkovskii, A. Melnikov, D. Michael, V. Milenin, S. Murashov, L. Rakcheeva, N. Timofeev, and G. Zissis, J. Phys. D: Appl. Phys. **42**, 175204 (2009).
[7]A. General and S. Avtaeva, Tech. Phys. **55**, 715 (2010).
[8]S. Avtaeva, A. General, and V. Kel'man, J. Phys. D: Appl. Phys. **43**, 315201 (2010).
[9]A. Shuaibov and A. Malinin, Uzhhorod Univ. Sci. Herald: Ser. Phys. **27**, 50 (2010).
[10]A. Shuaibov, A. Minya, A. Malinin, Z. Gomoki, and R. Gritzak, J. Appl. Spectrosc. **78**, 867 (2012).
[11]R. Hrytsak, N. Ilavska, and A. Shuaibov, Uzhhorod Univ. Sci. Herald: Ser. Phys. **29**, 227 (2011).
[12]D. Levko, A. Shuaibov, A. Minya, R. Gritzak, and Z. Gomoki, High Voltage Eng. **39**, 2193 (2013).
[13]A. N. Zavilopulo, A. I. Dolgin, and M. A. Khodorkovsky, Phys. Scr. **50**, 696 (1994).
[14]R. W. B. Pears and A. G. Gaydon, *The Identification of Molecular Spectra* (Chapman Hall LTD, London, 1963).
[15]D. X. Liu, P. Bruggeman, F. Iza, M. Z. Rong, and M. G. Kong, Plasma Sources Sci. Technol. **19**, 025018 (2010).